Impaired bioenergetics in mutant mitochondrial DNA determines cell fate during seizure-like activity

Stjepana Kovac [a,b*], Elisavet Preza [a], Henry Houlden [a], Matthew C. Walker [a], Andrey Y. Abramov [a,**]

[a] UCL Institute of Neurology, University College London, London, UK

[b] Department of Neurology, University of Muenster, Muenster, Germany

*Corresponding author:

Dr. Stjepana Kovac

Department of Neurology

University of Münster

Tel.: +49 (0) 251 83-44463

Fax: +49 (0) 0251 83-46812

Email: stjepana.kovac@ukmuenster.de

**Co-Corresponding author:

Prof. Andrey Y. Abramov

Department of Molecular Neuroscience

Tel.: +44 (0) 2078374062

Fax: +44 (0) 2078375069

Email : a.abramov@ucl.ac.uk

ABSTRACT

Mutations in genes affecting mitochondrial proteins are increasingly recognized in patients with epilepsy, but the factors determining cell fate during seizure activity in these mutations remain unknown.

Fluorescent dye imaging techniques were applied to fibroblast cell lines from patients suffering from common mitochondrial mutations and to an age matched controls. Using live cell imaging techniques in fibroblasts, we show that fibroblasts with mutations in the mitochondrial genome had reduced mitochondrial membrane potential and NADH pools and higher redox indices, indicative of respiratory chain dysfunction. Increasing concentrations of ferutinin, a Ca^{2+} ionophore, led to oscillatory Ca^{2+} signals in fibroblasts resembling dynamic Ca^{2+} changes that occur during seizure-like-activity. Co-monitoring of mitochondrial membrane potential ($\Delta\Psi_m$) changes induced by ferutinin showed accelerated membrane depolarization and cell collapse in fibroblasts with mutations in the mitochondrial genome when compared to controls. Ca^{2+} flash photolysis using caged Ca^{2+} confirmed impaired Ca^{2+} handling in fibroblasts with mitochondrial mutations.

Findings indicate that intracellular Ca^{2+} levels cannot be compensated during periods of hyperexcitability, leading to Ca^{2+} overload and subsequent cell death in mitochondrial diseases.

INTRODUCTION

Mutations in genes affecting mitochondrial proteins are increasingly recognized as a cause of human disease as genetic tools become more widely available in clinical practice (1). Although there is strong associational data between gene mutations and specific phenotypes, the functional consequences of these mutations remain less clear.

Mutations are not distributed evenly across the mitochondrial genome, but several hotspots exist. Such hotspots are seen in mitochondrial DNA coding for tRNA (2). The m.3243A>G MT-TL1 gene mutation and 8344A>G MT-TK gene mutation both affect tRNA and are frequently encountered in human disease. M.3243A>G MT-TL1 gene mutations present with mitochondrial encephalopathy with stroke-like episodes (MELAS). This particular mutation accounts for 80% of cases with MELAS (3). Similarly the 8344A>G MT-TK gene mutation is another hotspot and accounts for 80% of cases presenting with myoclonic epilepsy with ragged red fibres (MERRF) (4).

A common feature in mitochondrial disease, and also in the two above described syndromes, is network hyperexcitability leading to seizures. Indeed, epilepsy is an important aspect of mitochondrial disease and contributes significantly to morbidity (5, 6).

We have previously shown that hyperexcitability in cellular epilepsy models affects Ca^{2+} handling in mitochondria and ROS homeostasis, ultimately altering energy homeostasis in neurons (7, 8). It is possible that similar mechanisms apply to hyperexcitability and seizures seen in patient suffering from mitochondrial mutations, but such evidence is lacking.

One approach to address these questions would be to create networks of neurons from reprogrammed cell lines. However, there are problems inherent to cell reprogramming including determining cell identity and generating networks that can maintain seizure-like activity.

Several lines of evidence suggest that calcium handling is impaired in different types of cells with mitochondrial mutations and not only in neurons (9, 10). This is not

surprising, and is likely due to the fact that mitochondrial calcium handling is a process which is conserved among vertebrate species and more importantly between different tissues (11). It implies that mitochondrial pathologies and functions can be studied in different tissues. This is supported by a study investigating neurons derived from various 'cybrid' embryonic stem cell lines harboring mutations in complex I and IV (10). Interestingly this study found similar calcium-handling deficits in neurons and fibroblasts of patients with MELAS syndrome, suggesting that the cellular pathology in mitochondrial disease might be reflected in many different cell types but also in fibroblasts and thus fibroblasts seem to faithfully reproduce the disease phenotype.

We have thus taken an alternative approach that is robust, and easy to implement and so lends itself to large-scale drug screening. In this study we determined the mechanisms underlying impaired Ca^{2+} handling in mitochondrial disease using human fibroblasts as a disease model. Human fibroblasts have a different system of ion channels participating in signal transmission. To address this, we induced large intracellular Ca^{2+} transients (such as those occurring during seizure activity) in these cells using Ca^{2+} ionophores and caged Ca^{2+}.

RESULTS

Identification of mitochondrial pathology in patients' fibroblasts

The mitochondrial membrane potential ($\Delta\Psi_m$) is a universal indicator of mitochondrial integrity and function. Alterations of $\Delta\Psi_m$ are a marker of mitochondrial disease pathology. We therefore compared basal $\Delta\Psi_m$ in fibroblasts with mitochondrial mutations to those of age matched controls. There was a statistically significant difference in the ΔΨm ($\Delta\Psi_m$) between the groups as measured with TMRM ($F(4,23) = 6.380$; $p<0.01$; one way ANOVA; Fig. 1A). ΔΨm was ~15-20% lower in t-RNA mutations (MT-TL1 and MT-TK) and ~40% lower in complex one mutation (MT-ND5) when compared to that in control (C).

Next we investigated how robust ΔΨm is in fibroblasts when challenged with oligomycin and rotenone, potent inhibitors of mitochondrial complex V and I. This

was done by assessing the drop in TMRM fluorescence, and thus the degree of depolarization of the mitochondrial membrane potential after application of oligomycin and rotenone. To assess the functional reserve of the ΔΨm the mitochondrial uncoupler carbonylcyanide-p-trifluoromethoxyphenylhydrazone (FCCP; 1 µM) was added after application of those inhibitors, which in all experiments led to complete depolarization of ΔΨm, i.e. loss of TMRM fluorescence (Fig. 1 B and C). There was a statistically significant difference in the magnitude of $\Delta\Psi_m$ drop (Δ TMRM) between the different cell lines after addition of oligomycin (Fig. 1D, $F(4,166) = 30.95$; $p<0.001$; one way ANOVA), rotenone (Fig. 1E, $F(4,166) = 26.24$; $p<0.001$; one way ANOVA) and FCCP (Fig. 1F, $F(4,166) = 9.30$; $p<0.001$; one way ANOVA). Control cells showed only a mild drop in $\Delta\Psi_m$ of around 10% of the total mitochondrial membrane potential in response to the F_1F_0-ATP synthase inhibitor oligomycin (0.2 µg/ml; Fig. 1B and D), while mitochondria in mutated cells showed marked depolarization of $\Delta\Psi_m$ in response to oligomycin, ranging from 25%-70% (post hoc Dunnett's test; Fig. 1D). Subsequent inhibition of complex I by rotenone (5 µM) caused a rapid loss of potential which also differed in its magnitude between the cell lines (post hoc Dunnett's test; Fig. 1B, C, and F). Control cells showed the most marked depolarization after rotenone application reaching ~ 55% of $\Delta\Psi_m$, whereas in cells with mitochondrial mutations depolarization with rotenone was less pronounced ranging from ~ 20-45% (Fig.1F). This is likely due to the fact that in those cells inhibition of complex V with oligomycin already yielded a marked depolarization. Finally, the functional of $\Delta\Psi_m$ after complex I and complex V inhibition, as assessed with FCCP, showed also marked differences between the groups (post hoc Dunnett's test; Fig. 1B, C, and G). These findings imply that the ΔΨm in fibroblasts with the mitochondrial mutations is maintained by complex V working in reverse mode and thus at the expense of respiration and oxidative phosphorylation.

Basal NADH levels and redox index in fibroblasts with mitochondrial mutations

NADH is a complex I substrate. The redox index of NADH expresses the ratio of maximally oxidised and maximally reduced NADH states within the mitochondria. Maximal oxidation is stimulated by treatment with mitochondrial uncoupler 1 µM

FCCP. Maximal reduction is established by inhibiting respiration with 1mM NaCN (for examples see Fig. 2A and C). The redox state therefore is a measure of the activity of the mitochondrial electron transport chain.

We found that there was a statistically significant difference in the NADH levels between the different groups ($F(4,15) = 14.69$; $p<0.001$; one way ANOVA; Fig. 2 B). The reduction in NADH levels varied between ~80% in fibroblasts with MT-ND5 mutations ($p=0.027$; post hoc Dunnett's test), ~70% in fibroblasts with MT-TL1 mutation ($p=0.003$; post hoc Dunnett's test) and was most prominent in fibroblasts with MT-TK mutations showing a reduction of ~40% ($p<0.001$; post hoc Dunnett's test; Fig. 2B) compared to control. There was no difference between the control and the fibroblasts from the unaffected mother (MT-TK_c). The reduction in mitochondrial NADH pool may be explained by higher consumption of NADH via complex I or by a slower rate of production of this molecule in the TCA cycle. Thus, we next established the redox indexes. In a one way ANOVA we found a significant difference in the redox index between the groups ($F(4,18) = 3.60$; $p<0.05$). The redox index was increased when compared to control. This increase varied from ~15-30%. Post hoc analysis revealed that this reached statistical significance for fibroblasts harbouring the MT-TK mutation ($p=0.007$; post hoc Dunnett's test; Fig. 2D). Increased redox index indicates lower activity of the complex I activity in fibroblasts with mitochondrial mutation confirming their impaired respiration. Lower NADH pools in cells harbouring mitochondrial mutations when compared to control cells and decreased activity of complex I related respiration as expressed by the redox index suggests partial inhibition of NADH production in TCA cycle.

Mitochondrial mass

Mitochondrial dysfunction and energy deprivation in some cells can be compensated by increased mitochondrial biogenesis. However, there was no statistically significant difference in the mitochondrial mass between fibroblasts with different mitochondrial mutations and controls ($F(4,17) = 14.73$; $p=0.194$; one way ANOVA). Mitochondrial mass varied between 9 and 14 volume percent of the cell and was highest in the MT-TKc mutation suggesting some compensatory effect of mitochondrial mass (Suppl. Fig. 1).

Dynamic Ca^{2+} handling in cells with mitochondrial mutations

Network hyperexcitability in mitochondrial disease can result in seizures and epilepsy. Such hyperexcitability is critically dependent on Ca^{2+} homeostasis within the cell with the mitochondria playing a major role in Ca^{2+} homeostasis (7, 12). Unsurprisingly, the mutations investigated here presented with seizures as a prominent phenotype (see Suppl. Table 1). We therefore investigated whether dynamic Ca^{2+} handling, which is required in situations with large intracellular Ca^{2+} rises as seen in seizures (7), is impaired in fibroblasts with mitochondrial mutations.

In addition, mitochondrial dehydrogenases (including NADH dehydrogenase) are calcium dependent enzymes (13). Mitochondrial calcium uptake regulates respiration and as result increases in mitochondrial calcium uptake lead to increased ATP production (14). In addition, mitochondrial calcium capacity is a key element in regulation of mPTP. We thus quantified mitochondrial calcium pools. We also quantified ER calcium pools since these are closely interlinked with mitochondrial calcium signalling (15). We estimated these by stimulating Ca^{2+} release from the endoplasmatic reticulum (ER) with 1 µM thapsigargin and subsequently by depleting mitochondrial Ca^{2+} with 1 µM ionomycin (Fig.3 A) in Ca^{2+} free external medium. We found a significant difference in ER Ca^{2+} pools as estimated by fura-2 ratios between the fibroblast cell lines ($F(4,475) = 19.14$; $p<0.001$; one way ANOVA). Similarly, mitochondrial Ca^{2+} pools varied significantly between the fibroblast cell lines ($F(4,476) = 33.07$; $p<0.001$; one way ANOVA). In fibroblasts with complex I mutation (MT-ND5) mitochondrial Ca^{2+} pools were smaller whereas ER Ca^{2+} pools were larger when compared to control (Fig.3 B and C). Interestingly, the reverse was observed with MT-TK mutations. MT-TL1 mutations did not show any differences in either ER or mitochondrial Ca^{2+} pools when compared to control.

We next explored different models to assess Ca^{2+} handling in fibroblasts with mitochondrial mutations. Unlike excitatory cells such as neurons, fibroblasts are cells specialized to synthesize extracellular matrix and as such lack the receptor composition found on neurons. We and others have highlighted a critical role of NMDA receptor mediated Ca^{2+} toxicity during seizure activity (7, 16).

We therefore sought to model repetitive Ca^{2+} changes using pharmacological tools. Ferutinin, a naturally occurring terpenoid, has Ca^{2+} ionophoretic properties by increasing cation permeability of cells and mitochondria in a dose-dependent manner (17, 18). Ferutinin therefore contributes to mitochondrial permeability transition pore (MPTP) opening via Ca^{2+} overload (19). We have previously found that MPTP opening contributes to neuronal cell death in hyperexcitability (7). We found that increasing concentrations of ferutinin lead to oscillatory Ca^{2+} signals in the cytosol (Fig. 4A, upper panel). These signals were accompanied by changes in the ΔΨm (Fig. 4A, lower panel). Qualitative analysis of the ΔΨm changes induced by increasing concentrations of ferutinin identified two distinct phases: (1) a phase which was characterized by a relative stable $\Delta\Psi_m$ or only minor $\Delta\Psi_m$ changes and (2) a time point with accelerated $\Delta\Psi_m$ changes (see Fig. 4A). This acceleration coincided with a steep increase in the Ca^{2+} signal (see fluo-4 trace) and could be visualized as either decrease of TMRM fluorescence as measured over mitochondria *or* increased TMRM fluorescence over the nuclei. The nuclei exhibit a transient increase of TMRM fluorescence once the dye is redistributed (Suppl. Fig. 2). We interpreted this steep decline in $\Delta\Psi_m$ as mitochondrial permeability transition pore (MPTP) opening. Comparison of different fibroblast cell lines showed that MPTP opening (phase 2), measured as peak fluorescence over cell nuclei differed ($F(4,82) = 23.23$; $p<0.001$; one way ANOVA). Post hoc analysis showed that this difference was sustained by a significantly accelerated MPTP opening in fibroblasts with complex I mutations (MT-ND5; $p<0.001$; Post hoc Dunnett's test; Fig. 4B). There was a trend toward earlier PTP opening in the MT-TK cell line when compared to control ($p=0.054$; Post hoc Dunnett's test). We next analysed the slope of TMRM fluorescence change measured over mitochondria representing the initial phase (phase 1) defined by a slow decline in $\Delta\Psi_m$. We found a significant difference between the cell lines ($F(4,102) = 13.64$; $p<0.001$; one way ANOVA, Fig. 4C). Post hoc analysis showed that there was a steep phase 1 decline in $\Delta\Psi_m$ of fibroblasts with complex one mutations (MT-ND5; $p<0.001$; Post hoc Dunett's test) and there was a trend in fibroblasts with MT-TK t-RNA mutations ($p=0.036$; Post hoc Dunnett's test) when compared to control (Fig. 4C-E).

To model repetitive Ca^{2+} oscillations in fibroblast - as those seen in neurons during seizure-like activity (Fig. 5A and B) - we loaded cells with the photolabile Ca^{2+} chelator *o*-nitrophenyl EGTA (NP-EGTA; caged Ca^{2+}). Upon UV exposure Ca^{2+} is released into the cell. We then studied the effect of Ca^{2+} challenge imposed by this technique on one mutation with a very profound effect (MT-ND5) and one with no effect (MT-TL1) on Ca^{2+} handling as assessed in the experiments with the Ca^{2+} ionophore ferutinin. We found that repetitive UV induced Ca^{2+} release in cells lead to a depolarization of the ΔΨm in /fibroblasts (Fig. 5E). This depolarization was not observed in adjacent cells not exposed to UV light (Fig. 5D). We applied this method to control fibroblasts and fibroblasts with MT-TL1 and MT-ND5 mutations. We found a steady decrease in the ΔΨm indicated by TMRM fluorescence decrease during Ca^{2+} flash photolysis (Fig. 6A) in cells harbouring mitochondrial mutations. This correlated to an increase in TMRM fluorescence over the nucleus. TMRM signals in nuclei were quantified given the difficulties measuring fluorescence over single mitochondria due to movement. There was a statistically significant difference in mitochondrial membrane potential depolarisation after repetitive Ca^{2+} challenge between control fibroblasts (n=9 cells) and fibroblasts harbouring the MT-TL1 mutation (n=7; $p<0.001$; t-test) or fibroblasts harbouring the MT-ND5 mutation (n=7; $p<0.001$; t-test; Fig. 6 B-E).

ATP depletion in fibroblasts with mitochondrial mutations

Mitochondrial Ca^{2+} uptake is electrogenic and thus leads to a depolarization of the mitochondrial membrane potential. The mitochondrial membrane potential is the driving force of ATP production and is dependent on a hyperpolarized mitochondrial membrane potential. Taken together this suggests that mitochondrial Ca^{2+} uptake is an energy depleting process.

Previously we demonstrated that Ca^{2+} oscillations induced by low Mg^{2+} seizure-like activity led to energy deprivation and cell death (7).

To investigate whether metabolic changes observed in fibroblasts with mitochondrial mutations are linked to ATP depletion, we investigated ATP levels measured with MAG fura after challenging fibroblasts with ferutinin in a glucose deprived environment. Fibroblasts are glycolytic cells whilst neurons are not. Thus, we made

use of glucose deprivation of the external medium to eliminate glycolysis as a source of ATP production, to be able to focus on mitochondrial ATP production. MAG fura allows real-time imaging of changes in ATP as intracellular magnesium concentrations are closely linked to ATP levels - free $[Mg^{2+}]_c$ increases during ATP depletion through hydrolysis of Mg^{2+}ATP (20). We first determined threshold concentrations of ferutinin which would lead to ATP depletion in fibroblasts. Stepwise increases in ferutinin concentration showed that 40-50 µM was the concentration required to induce rapid ATP changes in fibroblasts in a glucose deprived environment (Fig. 7A and B). We then measured the delay in ATP depletion after application of 40 µM ferutinin in the different fibroblast cell lines. In a one way ANOVA we found a significant difference in the delay to ATP depletion ($F(4,211) = 23.8$; $p<0.001$). Post hoc analysis revealed that fibroblasts harbouring the MT-TK mutation had faster ATP depletion compared to the other cell lines ($p<0.001$; post hoc Dunnett's test; Fig. 7C, D and E).

DISCUSSION

Studying mitochondrial function and the impact of disease pathophysiology on mitochondrial function is a challenge. We developed an experimental approach to study mitochondrial function during dynamic Ca^{2+} changes such as the ones observed during seizures and epilepsy. We here show that fibroblasts harbouring mutations in the mitochondrial genome have impaired ability to handle Ca^{2+} in these models. This may explain why, particularly during periods of hyperexcitability, intracellular Ca^{2+} levels cannot be compensated, leading to Ca^{2+} overload and subsequent cell death in these diseases.

Mitochondrial membrane potential in cells harbouring mitochondrial DNA mutations

We found decreased mitochondrial membrane potentials in fibroblasts harbouring mitochondrial DNA mutations. Previous studies have confirmed this showing decreases in $\Delta\Psi m$ in MT-TL1 and MT-TK mutations (21) and in ND6 point mutations (22). Under pathological conditions such as seen in anoxia, complex V works in a reverse mode thus maintaining $\Delta\Psi m$ at the expense of ATP consumption (21, 23).

Under these circumstances, blocking complex V with oligomycin depolarizes the ΔΨm. We have shown that this also applies to the mitochondrial mutations studied here. Whereas such reverse function of complex V has been observed in mtDNA cybrid mitochondria harbouring mutation in the ND5 gene (22) we expand this to include fibroblasts with the same mutation in the ND5 gene and 8344A>G mutation in tRNA. Both a lower ΔΨm and reverse mode functioning of complex V with ATP consumption in cells with mtDNA mutations are factors that should render these cells more vulnerable to Ca^{2+}-induced cell death and mitochondrial permeability transition pore opening. To confirm deficient oxidative phosphorylation in fibroblasts harbouring mtDNA mutations, we looked at NADH/NAD^+ ratios (redox indexes) reflecting the activity of the mitochondrial electron transport chain. We found decreased redox indices in cells harbouring mitochondrial mutations reflecting a deficiency of NADH to enter the electron transport chain. Despite this, NADH pools were low and NADH did not accumulate. This is likely to reflect an increase in glycolysis with transformation of pyruvate to lactate consuming NADH. Increased glycolysis has been observed previously in cybrids from the patient suffering from mitochondrial disease due to ND5 gene mutation (22) and have been used as a – albeit unspecific- marker in the evaluation of mitochondrial disease in patients (24). This glycolytic shift is also supported by previous data showing a decrease in mitochondrial respiration accompanied by increased glycolysis in fibroblasts with mitochondrial mutations as measured with the seahorse technology (25). Decreased energetic substrates might fuel mitochondrial biogenesis and we therefore asked whether the mitochondrial pool differed between the cell lines. There was no difference between the mitochondrial mass between the different fibroblasts. In keeping with our observations, James and colleagues found similar proportions of cell protein that sedimented in the mitochondrial fraction in fibroblast harbouring mitochondrial mutations (MELAS and MERRF) and control fibroblasts (21). In addition our results of ~10-15 % of total cell mass occupied by mitochondria parallels their and previous findings (21, 26).

$[Ca^{2+}]_c$ stores in cells harbouring mitochondrial DNA mutations

We found differences in ER and mitochondrial calcium pools between the mutations (Fig. 3) which could be explained by the fact that calcium handling is not only

determined by defects of oxidative phosphorylation, but also depend on the site of the dysfunction and the severity of the defect. Interestingly, the MT-ND5 mutation which is characterized by a severe impairment in Complex I showed decreased mitochondrial calcium stores whereas the tRNA mutations (MT-TL1 and MT-TK) showed increased mitochondrial calcium stores. There are links from the literature demonstrating that different mutations affect the complexes differentially. E.g. the MT-TL1 mutation results in respiratory defect arising from complex I and complex IV (27) whereas MT-TK mutation studied here has been shown to lead to a marked defect in overall mitochondrial translation (27, 28). This may explain different phenotypical manifestations and also different effects on calcium handling which were found in this study.

$[Ca^{2+}]_c$ challenge has different effects on the mitochondrial membrane potential, PTP opening and ATP depletion induced cell collapse in cells harbouring mitochondrial DNA mutations and controls

In normal cell metabolism NADH dehydrogenase (Complex I) can be stimulated by small concentrations of Ca^{2+}, leading to an increase in NADH turnover and thus hyperpolarisation of the ΔΨm (14, 29). We found that a stepwise increase in the intracellular Ca^{2+} concentration through ferutinin leads to a depolarisation of the ΔΨm, whereas an increase or a steady ΔΨm was observed in controls (Fig.4). Ca^{2+}-induced stepwise depolarisation of the ΔΨm was most evident in MT-ND5 fibroblast cell line, a mutation in the NADH dehydrogenase itself. Previous studies in the same cell line have suggested that this defect does not affect NADPH oxidase function itself but rather result in deficiency in proton pumping across the inner mitochondrial membrane (22). This decrease in $\Delta\Psi_m$ was present – albeit to a lesser degree - in fibroblast MT-TL1 and MT-TK mutations supporting previous reports (21). A more compromised $\Delta\Psi_m$ implies more severe pathology which is in keeping with the clinical observation that mutations in the NADH dehydrogenase present with a more severe phenotype including epilepsy in their presentation (22, 30). In addition we were able to replicate this using Ca^{2+} flash photolysis.

Further, previous reports show that the A3243G mutation disrupts 5-taurinomethyluridine (lacked τm5U modification) in mitochondrial tRNA leading to

UUG codon specific decoding difficulties. UUG codon usage in the 13 proteins encoded by mtDNA is low, with one exception, namely ND6 gene encoding complex I contains 8 UUG codons which form 42% of total ND6 codons in ND6 (31, 32). This explains why complex I translation is markedly reduced in this mutation whereas other mitochondrial complexes or proteins are relatively preserved (27, 31). Our data show that the ΔΨm after Ca^{2+}-challenge of fibroblasts with the A3243G mutation, remained relatively stable and the time point of PTP opening was comparable to control cell lines. This may be explained by a partially functional complex I and also by possible compensation by other complexes which maintain the ΔΨm.

Mutations in tRNALys such as A8344G, on the other hand, severely disrupt protein synthesis of several proteins involved in oxidative phosphorylation (27, 28, 33). This graded insufficient mitochondrial protein expression with ND6 mutations at the severe end of the spectrum, followed by 8344A>G mutation (MT-TK fibroblasts) and by 3243A>G mutations (MT-TL1 fibroblasts) presenting partial complex 1 deficiency, is mirrored in our findings of graded ΔΨm decrease with increasing Ca^{2+} challenge (Fig.5). Differences in MTPT opening indicated by rapid loss of ΔΨm were only observed in the MT-ND5 fibroblast cell line which showed rapid ΔΨm decline after repeated Ca^{2+} challenges, indicating that a critical depolarisation needs to be reached prior to MPTP opening (Fig.5B). It should be noted that differences in Ca^{2+} handling were picked up with Ca^{2+} flash photolysis in the MT-TL1 mutation which may point to different sensitivities of these models which as such may be used complementary.

Interestingly, the MT-TK cell line (A8344G) was characterised by high ATP consumption. This can be explained by FiF0ATPase working in reverse mode which is confirmed by the fact that oligomycin leads to a marked depolarization of the mitochondrial membrane potential in these cells (Fig.1C and D). In addition this cell line shows very low NADH pools (Fig. 2B) and high mitochondrial calcium (Fig. 3C). Taken together all these changes predispose to ATP depletion and cell collapse in the experiments performed (Fig. 7).

It is well known that lowering of the mitochondrial potential and ATP depletion can lead to lowering of the threshold of PTP opening and thereby increase the risk of Ca^{2+} induced cell death (34). The changes modelled here, therefore may serve as an

explanation for enhanced neuronal cell death in patients suffering from epilepsies due to mitochondrial mutations (35). Excessive Ca^{2+} oscillations, which are the cellular signature of epileptiform activity, impose a metabolic burden on the cell (7). This is due to mitochondrial Ca^{2+} buffering which competes with ATP generation and due to the need to restore cellular Ca^{2+} homeostasis, a process which is dependent on energetic molecules such as ATP. We here show that such oscillations induce mitochondrial membrane potential changes, which ultimately may lead to cell death, more readily in cells which are affected by mitochondrial mutations. This provides an insight into mechanisms of cell death in these conditions. More recently mutations in the mitochondrial genome have been identified in tissue samples from patients suffering from common types of epilepsy such as hippocampal sclerosis (36) which may indicate that these mechanisms also apply to more common epilepsy syndromes. In addition to mechanistic insight into disease processes, the models developed here may serve as screening tools for future drug development.

MATERIAL AND METHODS

Fibroblast lines

A total of five fibroblast cell lines were used for this study. Three fibroblast lines were generated from biopsies taken following patients' informed consent and ethical approval from the National Hospital for Neurology and Neurosurgery / Institute of Neurology Joint Research Ethics Committee (London, UK). The other two fibroblast lines were kindly provided by the MRC Centre for Neuromuscular Diseases BioBank London. The study lines included control fibroblasts (C), fibroblasts with the 3243A>G mutation in mitochondrial encoded tRNA leucine 1 (UUA/G) (MT-TL1), 13528A>G and 13565C>T mutations in mitochondrial encoded NADH dehydrogenase 5 (MT-ND5), 8344A>G mutation in mitochondrial encoded tRNA lysine (MT-TK) and finally fibroblasts from the unaffected mother of the MT-TK patient that serve as control (MT-TKc). Patients' clinical details are available in Suppl. Table 1. The rationale for choosing these mutations was that these mutations are a leading cause for mitochondrial disease and are the main mutations found in Mitochondrial encephalomyopathy, lactic acidosis, and stroke-like episodes (MELAS) and

Myoclonic epilepsy with ragged-red fibres (MERRF). Half of the pathogenic mutations in mtDNA map to mtRNA genes (37). The mutation 3243A>G accounts for 80% of patients suffering from MELAS (3, 38) and results in a translational depression of the ND6 (a subcomplex of complex I of the respiratory chain and thus explains decrease in complex I activity seen in these patients (32). In addition, the mutation 13528A>G and 13565C>T, whereas rare, is known to affect ND5 subunit of complex I (MT-ND5). Fibroblasts of this patient have been studied before (22). Mutation load in the mother's fibroblasts is 44 % compared to mutation load in the patient which is 82 %. Quantification of the proportion of the mutant mtDNA for each fibroblast cell line is presented in Suppl. Table 1. We want to highlight that the methods used in this paper rely on analyses of single cells and single mitochondria. Thus it is expected that these methods are more sensitive than conventional enzyme assays which are usually done in cell suspensions. Thus even low levels of mutation load are likely to translate into biological effects seen via live cell imaging. In addition, a previous study which investigated the effects of MT-TL1 mutation on mitochondrial membrane potential has confirmed this, showing that a low mutation load (of <50%) had an impact on the mitochondrial membrane potential (21).

Fibroblast cultures

Fibroblast lines were generated from ~4mm punch biopsies taken under local anaesthesia (1-2 ml of 1 % lidocaine) following informed consent. Biopsies were dissected and cultivated in 5cm petri dishes in Dulbecco's modified Eagle's medium (DMEM-Glutamax, Invitrogen) supplemented with 10% FBS and 1% (v/v) penicillin/streptomycin at 37 °C in 5% CO_2 humidified, to allow fibroblast outgrowth. Once fibroblasts reached confluency, cells were detached with TrypleE (Invitrogen), transferred to T75 tissue culture flasks for further expansion and cryopreservation.. For all experiments fibroblasts were plated onto 22 mm coverslips 24h prior to experiments. All cells were kept at a comparable passage number (±2 passages) and experiments were always run in parallel with control. All experiments were normalized to control (C).

Measurement of mitochondrial membrane potential ($\Delta\Psi_m$)

Fibroblasts were loaded with 25 nM tetramethyl rhodamine methyl ester (TMRM) in a HEPES-buffered salt solution (HBSS, Invitrogen). Cells were incubated for 50 minutes prior to experiments to allow for equilibration of TMRM which is achieved late into the incubation process. This concentration of TMRM allows imaging of TMRM in “redistribution mode” and thus a reduction in mitochondria localized TMRM fluorescence represents mitochondrial depolarization. At the same time reduction of the TMRM fluorescent signal leads to a mild increase in TMRM cytosolic signal due to redistribution of the dye. This redistribution also occurs across the plasma membrane, and thus an initial rise of cytosolic TMRM is followed by a slow steady decline due to redistribution across the plasma membrane (Suppl. Fig.2). This redistribution kinetic allows visualizing the velocity of TMRM redistribution by plotting the cytosolic TMRM fluorescence changes. A peak of the TMRM signal thus indicates fastest TMRM redistribution and therefore was taken as an indicator of permeability transition pore opening in our experiments (Suppl. Fig. 2). The dye was kept in the solution throughout the experiment. Confocal images were acquired using a Zeiss 710 VIS CLSM (Zeiss, Oberkochen, Germany) equipped with a META detection system and a ×40 oil immersion objective. Excitation of the dye was through the 560nm laser and fluorescence was measured above 580nm. For all experiments, the confocal microscope illumination intensity was kept to a minimum (at 0.2% of laser output) to avoid phototoxicity and the pinhole was set to give an optical slice of ~2 µm. TMRM fluorescence was measured over mitochondria only and is therefore independent of the mitochondrial mass or density. We automated choice of regions of interest within the mitochondria and automated removal of the background using *Volocity* 3D Image Analysis *Software* (Perkin, Elmer).

Basal $\Delta\Psi_m$ as shown in Fig.1 was measured by recording z-stacks images whereas the kinetic response of $\Delta\Psi_m$ to mitochondrial toxins as shown in Fig.1B-E was obtained as a time series recording in a single plane.

Measurement of NADH redox indices

An epifluorescence inverted microscope equipped with a × 20 fluorite objective was used to measure NADH autofluorescence. The microscope is fitted with a Xenon arc lamp and a monochromator (Cairn Research, Faversham, Kent, UK). Excitation light

for the experiments was 350nm and emission fluorescence was captured through a 455nm long-pass filter to a cooled CCD camera (Retiga, QImaging, Surrey, BC, Canada) and digitised to 12 bit resolution.

Measurement of mitochondrial mass

To determine the mitochondrial mass, cells were loaded with 25 nM TMRM and Cell Trace Calcein Blue AM (5μM, Invitrogen) and 0.005% Pluronic for 40 minutes. Z-stack Confocal images were acquired using a Zeiss 710 VIS CLSM (Zeiss, Oberkochen, Germany), equipped with a META detection system and a ×40 oil immersion objective. Excitation of the dye was through the 560nm laser for TMRM and 405 laser for calcein blue and fluorescence emission was measured above 580nm. Mitochondrial mass was computed as the ratio of the volume of the mitochondrial network (determined by TMRM fluorescence) divided by the volume of the fibroblast (determined as calcein blue fluorescence) expressed in percentage. Images were auto-contrasted separately to allow definition of the mitochondrial network independent of the ΔΨm. Volumes were determined using *Volocity* 3D Image Analysis *Software* (Perkin, Elmer).

Measurement of $[Ca^{2+}]_c$ pools

For measurements of mitochondrial and endoplasmatic Ca^{2+} pools, cells were loaded with fura-2 AM and 0.005% Pluronic in a HEPES-buffered solution. Fibroblasts were incubated for 30 minutes prior to experiments and experiments were performed in a Ca^{2+} free HEPES- buffered solution. $[Ca^{2+}]_c$ was measured in single fibroblasts using excitation light provided by a xenon arc lamp, the beam passing through a monochromator at 340 and 380 with bandwidth of 10nm (Cairn Research, Kent, UK). Emitted fluorescent light passed through a 515-nm long pass filter to a cooled CCD camera (Retiga; QImaging) and was digitized to 12-bit resolution. Ca^{2+}imaging data was acquired at a frame interval of 10 s and analyzed using software from Andor (Belfast, UK). Traces were computed and plotted as fura-2 ratio of excitation acquired at 340 and 380 nm, both with emission at >515 nm. Fura ratio was not calibrated due to inaccuracies arising from different calibration methods.

Co-measurements of $\Delta\Psi_m$ and $[Ca^{2+}]_c$ were performed using TMRM and fluo-4. TMRM staining method is explained above. Fibroblasts were incubated with TMRM and fluo-4 and 0.005% Pluronic in a HEPES-buffered solution for 40 min. Incubation solution was replaced with fresh HEPES-buffered solution and 25 nM TMRM prior to experiments. TMRM and fluo-4 fluorescence were measured on a confocal microscope using a 64x objective to allow visualization of single mitochondria. In addition to the laser settings required to capture TMRM fluorescence (see above), fluo-4 was excited with the 488 laser and emission light was measured at 505–550 nm.

Measurement of ATP levels and cell collapse as indicated by massive $[Ca^{2+}]_c$ increases

Kinetic ATP changes and massive $[Ca^{2+}]_c$ in fibroblasts were determined indirectly by measuring free intracellular $[Mg^{2+}]_c$ and free intracellular $[Ca^{2+}]_c$ simultaneously. Mg^{2+} is released from Mg^{2+}-ATP due to consumption of ATP and therefore Mg^{2+} increase can be seen as a surrogate marker of intracellular ATP decrease. To measure $[Mg^{2+}]_c$ we used the ratiometric dye MAG-fura (Invitrogen). MAG-fura is a high affinity Mg^{2+} indicator and a low affinity Ca^{2+} indicator. This is critical since in situations with massive ATP depletion ionic homeostasis will be affected, resulting in a Ca^{2+} overload of the cell. This will result in a massive increase in MAG-fura fluorescence signifying an energetic collapse of the cell. We made use of this dual function of MAG fura, i.e. measurement of basal ATP levels and energetic collapse (see Fig.8). Fibroblasts were incubated with MAG fura AM and 0.001% pluronic for 30 minutes prior to experiments. Fluorescent images were obtained with the same settings as outlined for fura-2 AM measurements and expressed as ratios (340/380 MAG fura ratio). The delay to energetic collapse was determined for each fibroblast by determining the x-coordinate (time) of the maximum slope of the MAG-fura signal (see Fig.8).

Ca^{2+} flash photolysis

For imaging of $\Delta\Psi_m$ and Ca^{2+} during flash photolysis a Zeiss 510 UV–vis CLSM equipped with a META detection system and a X40 oil immersion objective was

used. Caged Ca^{2+}, 10 µM *o*-nitrophenyl EGTA, AM (NP-EGTA, AM) was incubated at the same time as fluo-4 and TMRM , and Ca^{2+}-free medium containing 0.5 mM EGTA (39). Flashes were delivered to a region of interest, which was defined prior to the experiments, targeting single cells. Flashes were delivered at a rate of 1 flash per minute. Ca^{2+} increase was verified by recording qualitative Ca^{2+} changes with fluo-4. Excitation and emission spectra were similar as those outlined above for TMRM and fluo-4.

Statistical analyses

Statistical analyses (one way ANOVA, Dunnett's test) were performed using SPSS 17.0 (Chicago, IL, USA). The significance level was set at $p < 0.05$ and all data are given as mean ± standard error of the mean (SEM). Post hoc calculations were computed to compare the difference to control (C).

Author contributions

SK and AYA conceived the study. SK performed and designed the experiments. EP and HH contributed towards the experiments. SK and AYA analysed the data. SK, AYA and MCW wrote the manuscript. All authors critically discussed the data and approved the final version of the manuscript.

Acknowledgments

The authors would like to thank the MRC Centre for Neuromuscular Diseases BioBank London for providing additional fibroblast lines for this study. This work was supported by the NIHR Queen Square Dementia Biomedical Research Unit. This work was undertaken at UCLH/UCL which receives a proportion of funding from the Department of Health's NIHR Biomedical Research Centres funding scheme.

LEGENDS OF FIGURES

Figure 1: Mitochondrial membrane potential in fibroblasts with mitochondrial mutations

Mitochondrial membrane potential ($\Delta\Psi_m$) is depolarized in fibroblast cell lines harbouring mitochondrial mutations when compared to control cell lines (A) and $\Delta\Psi_m$ is maintained at the expense of respiration in some mitochondrial mutations (B-E). Representative experiments from control (B) fibroblasts, fibroblasts from unaffected mother (MT-TKc; D) and fibroblasts harbouring mitochondrial mutations (C and E; MT-ND5 and MT-TK). Data indicate mean and SEM of TMRM fluorescence in fibroblasts in a representative experiment. Traces are normalized with 100% set as baseline TMRM fluorescence and 0% set as fluorescence after complete depolarization of $\Delta\Psi_m$ with FCCP. Note that oligomycin profoundly decreases TMRM fluorescence in mitochondrial mutations (C and E) whereas this effect is not visible in control fibroblasts/ fibroblasts from the unaffected parent (B and D). ΔΨm is expressed as TMRM fluorescence. High TMRM fluorescence intensities indicate relative hyperpolarization whereas low fluorescence indicates depolarization. Data is normalized to the control (C) cell line. Note that $\Delta\Psi_m$ is reduced in fibroblasts with mitochondrial mutations (MT-TL1; MT-ND5 and MT-TK) when compared to control (C), but not in fibroblasts from the unaffected mother (MT-TKc). Error bars indicate SEM. $^{**}p < 0.01$

Figure 2: NADH pools are low and NADH redox indices are decreased in fibroblasts with mitochondrial mutations suggesting inhibition of respiration

NADH autofluorescence was measured after supramaximal stimulation of respiration with FCCP and inhibition of respiration with NaCN (A and C). NADH pools were determined as the magnitude of fluorescence change between supramaximal stimulation and inhibition of respiration (A). Bar charts showing mean (± SEM) NADH pools of the fibroblast cell lines (B). Data normalized to control (set as 100%). Redox indices were determined as ratio of maximally oxidised and maximally reduced

NADH states and can be determined after supramaximal stimulation of respiration with FCCP and inhibition of respiration with NaCN. Redox indices are given in %. Bar chart comparing mean (± SEM) redox indices (D). Panel A and C show representative experiments. Traces in A and C represent mean and SEM of fibroblasts within one experiment. Note that NADH pools are reduced in fibroblast cell lines with mitochondrial mutations and that redox indices are high, indicating deficient respiration.

Figure 3: Mitochondrial Ca^{2+} stores and reticular Ca^{2+} stores in different fibroblasts cell lines

Method used to estimate cellular Ca^{2+} stores (A). Each trace represents cytoplasmic Ca^{2+} measurements in single fibroblasts. Ca^{2+} stores were estimated in Ca^{2+} free media by adding thapsigargin (1 µM) to estimate reticular Ca^{2+} stores and by adding ionomycin (1µM) to measure mitochondrial Ca^{2+} stores. Bar charts summarizing reticular (B) and mitochondrial (C) Ca^{2+} stores as measured with fura-2.

Figure 4: Dynamic Ca^{2+} handling in fibroblasts with mitochondrial mutations

Ca^{2+} signal as measured with fluo-4 (A; upper panel) and corresponding $\Delta\Psi_m$ changes as measured with TMRM in fibroblasts (A; lower panel) after treatment with ferutinin in increasing concentrations. Each trace shown in A represents fluo-4 (upper panel) or TMRM (lower panel) signal measured in one fibroblast. Note that two distinct phases of TMRM signal can be distinguishes based on the shape of the signal. Phase 1 is characterized by a mild decrease in TMRM fluorescence. In phase 2, which coincides with an increase in intracellular Ca^{2+}, a rapid decrease in TMRM fluorescence is observed suggesting mitochondrial permeability transition pore (MPTP) opening. The ferutinin concentration used to initiate MPTP opening was considered the threshold concentration (* indicates this concentration). Bar chart summarizing mean (± SEM) threshold concentrations leading to MPTP opening in different fibroblast cell lines (data normalized to control; B). Bar chart summarizing mean (± SEM) slopes of TMRM fluorescence change in fibroblast cell lines (C). Representative traces of mean TMRM fluorescence during ferutinin application in control fibroblasts (D) and fibroblasts with mitochondrial mutation (MT-TK; E). ***$p < 0.001$

Figure 5: Modelling hyperexcitability induced dynamic Ca^{2+} changes in fibroblasts with caged Ca^{2+}

Phase contrast image of neurons in cultures (A upper panel) and repetitive Ca^{2+} oscillations measured in neurons during low magnesium treatment mimicking seizure like activity/ hyperexcitability in neurons (A lower panel). Each trace represents $[Ca^{2+}]_c$ changes in a single neuron as measured with fura-2. Fibroblasts in culture co-stained with fluo-4 and TMRM (B). Ca^{2+} oscillations are induced in fibroblasts loaded with caged Ca^{2+} via intermittent UV exposure triggering Ca^{2+} released. This Ca^{2+} release can be monitored by fluo-4. The trance in C represents Ca^{2+} changes in a single fibroblast intermittently exposed to UV light. Arrows indicate time points when fibroblasts were exposed to UV light. Traces in panel E represent repetitive Ca^{2+} oscillations (green trace, fluo-4) and $\Delta\Psi_m$ changes (red trace, TMRM) in a single fibroblast triggered by UV (E). Note that UV induced Ca^{2+} oscillations in fibroblasts (E) resemble those seen in neurons during seizure like activity (A lower panel). Repetitive Ca^{2+} oscillations trigger $\Delta\Psi_m$ depolarisation in fibroblasts (E), whereas fibroblasts not stimulated with UV light do not show $\Delta\Psi_m$ depolarisation (D).

Figure 6: Impact of seizure-like oscillatory Ca^{2+} changes on mitochondrial membrane potential in cells harbouring mitochondrial mutations

Decrease in TMRM fluorescence measured over mitochondria after repetitive Ca^{2+} challenge (A). TMRM fluorescence measured over cell nuclei shows a slight increase in control cells (B) whereas a significant increase was noted in cells harbouring mitochondrial mutations (C, D) indicating redistribution of the dye from depolarized mitochondria. Histogram quantifying increase of TMRM fluorescence over nuclei in control cells and cells harbouring mitochondrial mutations (E).

Figure 7: ATP depletion in fibroblasts with mitochondrial mutations

Increasing concentrations of ferutinin in glucose free media lead to ATP depletion in fibroblast reflected by $[Mg^{2+}]_c$ increase. Traces in A-D represent MAG fura signal measured in a fibroblast. Each trace represents a fibroblast. Note that in control fibroblasts (A) lower ferutinin concentrations are required to induce ATP depletion when compared to fibroblasts harbouring the MT-TK mutation. Note that at the end of the 30 min interval captured some control fibroblasts have not shown significant ATP

depletion (A) whereas almost all fibroblasts with MT-TK mutation showed significant ATP depletion. Applying a single dose of ferutinin (40 µM) leads to ATP depletion in control fibroblasts (C) after a delay and immediate ATP depletion in fibroblasts harbouring the MT-TK mutation (D). Bar chart summarizing (± SEM) delay in ATP depletion as measured by MAG fura in different fibroblast cell lines (E).

Supplementary Figure 1: Mitochondrial mass

Bar chart summarizing mitochondrial mass in different fibroblast cell lines. Mitochondrial mass is expressed as mitochondrial volume / total cell volume (%).

Supplementary Figure 2: Method used to determine MTPT opening in fibroblasts treated with ferutinin

Traces represent mean (± SEM) TMRM fluorescence changes measured over mitochondria (solid triangles) and the nucleus (open triangle). Fluorescence measured over mitochondria show depolarization of $\Delta\Psi_m$ in a stepwise fashion. Once a cumulative concentration of 13.5 µM ferutinin is reached, depolarization $\Delta\Psi_m$ is accelerated as suggested by the change in the slope of TMRM fluorescence. This change indicates mitochondrial permeability transition pore opening. Due to redistribution of the dye, this appears to coincide with peak TMRM fluorescence in the nucleus. Nuclear peak fluorescence was therefore used to determine MPTP opening.

REFERENCES

1. Schapira,A.H.V. (2012) Mitochondrial diseases. *Lancet*, **379**, 1825–1834.

2. Abbott,J.A., Francklyn,C.S. and Robey-Bond,S.M. (2014) Transfer RNA and human disease. *Front Genet*, **5**, 158.

3. Goto,Y., Nonaka,I. and Horai,S. (1990) A mutation in the tRNA(Leu)(UUR) gene associated with the MELAS subgroup of mitochondrial encephalomyopathies. *Nature*, **348**, 651–653.

4. Shoffner,J.M., Lott,M.T., Lezza,A.M., Seibel,P., Ballinger,S.W. and Wallace,D.C. (1990) Myoclonic epilepsy and ragged-red fiber disease (MERRF) is associated with a mitochondrial DNA tRNA(Lys) mutation. *Cell*, **61**, 931–937.

5. Schapira,A.H.V. (2006) Mitochondrial disease. *Lancet*, **368**, 70–82.

6. Canafoglia,L., Franceschetti,S., Antozzi,C., Carrara,F., Farina,L., Granata,T., Lamantea,E., Savoiardo,M., Uziel,G., Villani,F., *et al.* (2001) Epileptic phenotypes associated with mitochondrial disorders. *Neurology*, **56**, 1340–1346.

7. Kovac,S., Domijan,A.-M., Walker,M.C. and Abramov,A.Y. (2012) Prolonged seizure activity impairs mitochondrial bioenergetics and induces cell death. *J. Cell. Sci.*, **125**, 1796–1806.

8. Kovac,S., Domijan,A.-M., Walker,M.C. and Abramov,A.Y. (2014) Seizure activity results in calcium- and mitochondria-independent ROS production via NADPH and xanthine oxidase activation. *Cell Death Dis*, **5**, e1442.

9. Moudy,A.M., Handran,S.D., Goldberg,M.P., Ruffin,N., Karl,I., Kranz-Eble,P., DeVivo,D.C. and Rothman,S.M. (1995) Abnormal calcium homeostasis and mitochondrial polarization in a human encephalomyopathy. *Proc. Natl. Acad. Sci. U.S.A.*, **92**, 729–733.

10. Trevelyan,A.J., Kirby,D.M., Smulders-Srinivasan,T.K., Nooteboom,M., Acin-Perez,R., Enriquez,J.A., Whittington,M.A., Lightowlers,R.N. and Turnbull,D.M. (2010) Mitochondrial DNA mutations affect calcium handling in differentiated neurons. *Brain*, **133**, 787–796.

11. Carafoli,E. and Lehninger,A.L. (1971) A survey of the interaction of calcium ions with mitochondria from different tissues and species. *Biochem J*, **122**, 681–690.

12. Szabadkai,G. and Duchen,M.R. (2008) Mitochondria: the hub of cellular Ca2+ signaling. *Physiology (Bethesda)*, **23**, 84–94.

13. Denton,R.M., McCormack,J.G. and Edgell,N.J. (1980) Role of calcium ions in the regulation of intramitochondrial metabolism. Effects of Na+, Mg2+ and ruthenium red on the Ca2+-stimulated oxidation of oxoglutarate and on

pyruvate dehydrogenase activity in intact rat heart mitochondria. *Biochem. J.*, **190**, 107–117.

14. Nicholls,D.G. (2005) Mitochondria and calcium signaling. *Cell Calcium*, **38**, 311–317.

15. Rizzuto,R., Pinton,P., Carrington,W., Fay,F.S., Fogarty,K.E., Lifshitz,L.M., Tuft,R.A. and Pozzan,T. (1998) Close contacts with the endoplasmic reticulum as determinants of mitochondrial Ca2+ responses. *Science*, **280**, 1763–1766.

16. DeLorenzo,R.J. and Sun,D.A. (2006) Basic mechanisms in status epilepticus: role of calcium in neuronal injury and the induction of epileptogenesis. *Adv Neurol*, **97**, 187–197.

17. Abramov,A.Y., Zamaraeva,M.V., Hagelgans,A.I., Azimov,R.R. and Krasilnikov,O.V. (2001) Influence of plant terpenoids on the permeability of mitochondria and lipid bilayers. *Biochim. Biophys. Acta*, **1512**, 98–110.

18. Zamaraeva,M.V., Hagelgans,A.I., Abramov,A.Y., Ternovsky,V.I., Merzlyak,P.G., Tashmukhamedov,B.A. and Saidkhodzjaev,A.I. (1997) Ionophoretic properties of ferutinin. *Cell Calcium*, **22**, 235–241.

19. Abramov,A.Y. and Duchen,M.R. (2003) Actions of ionomycin, 4-BrA23187 and a novel electrogenic Ca2+ ionophore on mitochondria in intact cells. *Cell Calcium*, **33**, 101–112.

20. Abramov,A.Y. and Duchen,M.R. (2010) Impaired mitochondrial bioenergetics determines glutamate-induced delayed calcium deregulation in neurons. *Biochim. Biophys. Acta*, **1800**, 297–304.

21. James,A.M., Wei,Y.H., Pang,C.Y. and Murphy,M.P. (1996) Altered mitochondrial function in fibroblasts containing MELAS or MERRF mitochondrial DNA mutations. *Biochem J*, **318**, 401–407.

22. McKenzie,M., Liolitsa,D., Akinshina,N., Campanella,M., Sisodiya,S., Hargreaves,I., Nirmalananthan,N., Sweeney,M.G., Abou-Sleiman,P.M., Wood,N.W., *et al.* (2007) Mitochondrial ND5 gene variation associated with encephalomyopathy and mitochondrial ATP consumption. *J. Biol. Chem.*, **282**, 36845–36852.

23. Appleby,R.D., Porteous,W.K., Hughes,G., James,A.M., Shannon,D., Wei,Y.H. and Murphy,M.P. (1999) Quantitation and origin of the mitochondrial membrane potential in human cells lacking mitochondrial DNA. *Eur. J. Biochem.*, **262**, 108–116.

24. Mitochondrial Medicine Society's Committee on Diagnosis, Haas,R.H., Parikh,S., Falk,M.J., Saneto,R.P., Wolf,N.I., Darin,N., Wong,L.-J., Cohen,B.H. and Naviaux,R.K. (2008) The in-depth evaluation of suspected mitochondrial disease. *Mol. Genet. Metab.*, **94**, 16–37.

25. Invernizzi,F., D'Amato,I., Jensen,P.B., Ravaglia,S., Zeviani,M. and Tiranti,V. (2012) Microscale oxygraphy reveals OXPHOS impairment in MRC mutant cells. *Mitochondrion*, **12**, 328–335.

26. Rugolo,M. and Lenaz,G. (1987) Monitoring of the mitochondrial and plasma membrane potentials in human fibroblasts by tetraphenylphosphonium ion distribution. *J. Bioenerg. Biomembr.*, **19**, 705–718.

27. Suzuki,T., Nagao,A. and Suzuki,T. (2011) Human mitochondrial tRNAs: biogenesis, function, structural aspects, and diseases. *Annu. Rev. Genet.*, **45**, 299–329.

28. Enriquez,J.A., Chomyn,A. and Attardi,G. (1995) MtDNA mutation in MERRF syndrome causes defective aminoacylation of tRNA(Lys) and premature translation termination. *Nat. Genet.*, **10**, 47–55.

29. McCormack,J.G., Halestrap,A.P. and Denton,R.M. (1990) Role of calcium ions in regulation of mammalian intramitochondrial metabolism. *Physiol. Rev.*, **70**, 391–425.

30. Ravn,K., Wibrand,F., Hansen,F.J., Horn,N., Rosenberg,T. and Schwartz,M. (2001) An mtDNA mutation, 14453G-->A, in the NADH dehydrogenase subunit 6 associated with severe MELAS syndrome. *Eur. J. Hum. Genet.*, **9**, 805–809.

31. Dunbar,D.R., Moonie,P.A., Zeviani,M. and Holt,I.J. (1996) Complex I deficiency is associated with 3243G:C mitochondrial DNA in osteosarcoma cell cybrids. *Hum. Mol. Genet.*, **5**, 123–129.

32. Kirino,Y., Yasukawa,T., Ohta,S., Akira,S., Ishihara,K., Watanabe,K. and Suzuki,T. (2004) Codon-specific translational defect caused by a wobble modification deficiency in mutant tRNA from a human mitochondrial disease. *Proc. Natl. Acad. Sci. U.S.A.*, **101**, 15070–15075.

33. Yasukawa,T., Suzuki,T., Ishii,N., Ohta,S. and Watanabe,K. (2001) Wobble modification defect in tRNA disturbs codon-anticodon interaction in a mitochondrial disease. *EMBO J.*, **20**, 4794–4802.

34. Bernardi,P., Petronilli,V., Di Lisa,F. and Forte,M. (2001) A mitochondrial perspective on cell death. *Trends Biochem. Sci.*, **26**, 112–117.

35. Sparaco,M., Bonilla,E., DiMauro,S. and Powers,J.M. (1993) Neuropathology of mitochondrial encephalomyopathies due to mitochondrial DNA defects. *J. Neuropathol. Exp. Neurol.*, **52**, 1–10.

36. Gurses,C., Azakli,H., Alptekin,A., Cakiris,A., Abaci,N., Arikan,M., Kursun,O., Gokyigit,A. and Ustek,D. (2014) Mitochondrial DNA profiling via genomic analysis in mesial temporal lobe epilepsy patients with hippocampal sclerosis. *Gene*, **538**, 323–327.

37. Brandon,M.C., Lott,M.T., Nguyen,K.C., Spolim,S., Navathe,S.B., Baldi,P. and Wallace,D.C. (2005) MITOMAP: a human mitochondrial genome database--2004 update. *Nucleic Acids Res.*, **33**, D611-613.

38. Kobayashi,Y., Momoi,M.Y., Tominaga,K., Momoi,T., Nihei,K., Yanagisawa,M., Kagawa,Y. and Ohta,S. (1990) A point mutation in the mitochondrial tRNA(Leu)(UUR) gene in MELAS (mitochondrial myopathy, encephalopathy, lactic acidosis and stroke-like episodes). *Biochem. Biophys. Res. Commun.*, **173**, 816–822.

39. Gandhi,S., Wood-Kaczmar,A., Yao,Z., Plun-Favreau,H., Deas,E., Klupsch,K., Downward,J., Latchman,D.S., Tabrizi,S.J., Wood,N.W., *et al.* (2009) PINK1-associated Parkinson's disease is caused by neuronal vulnerability to calcium-induced cell death. *Mol. Cell*, **33**, 627–638.

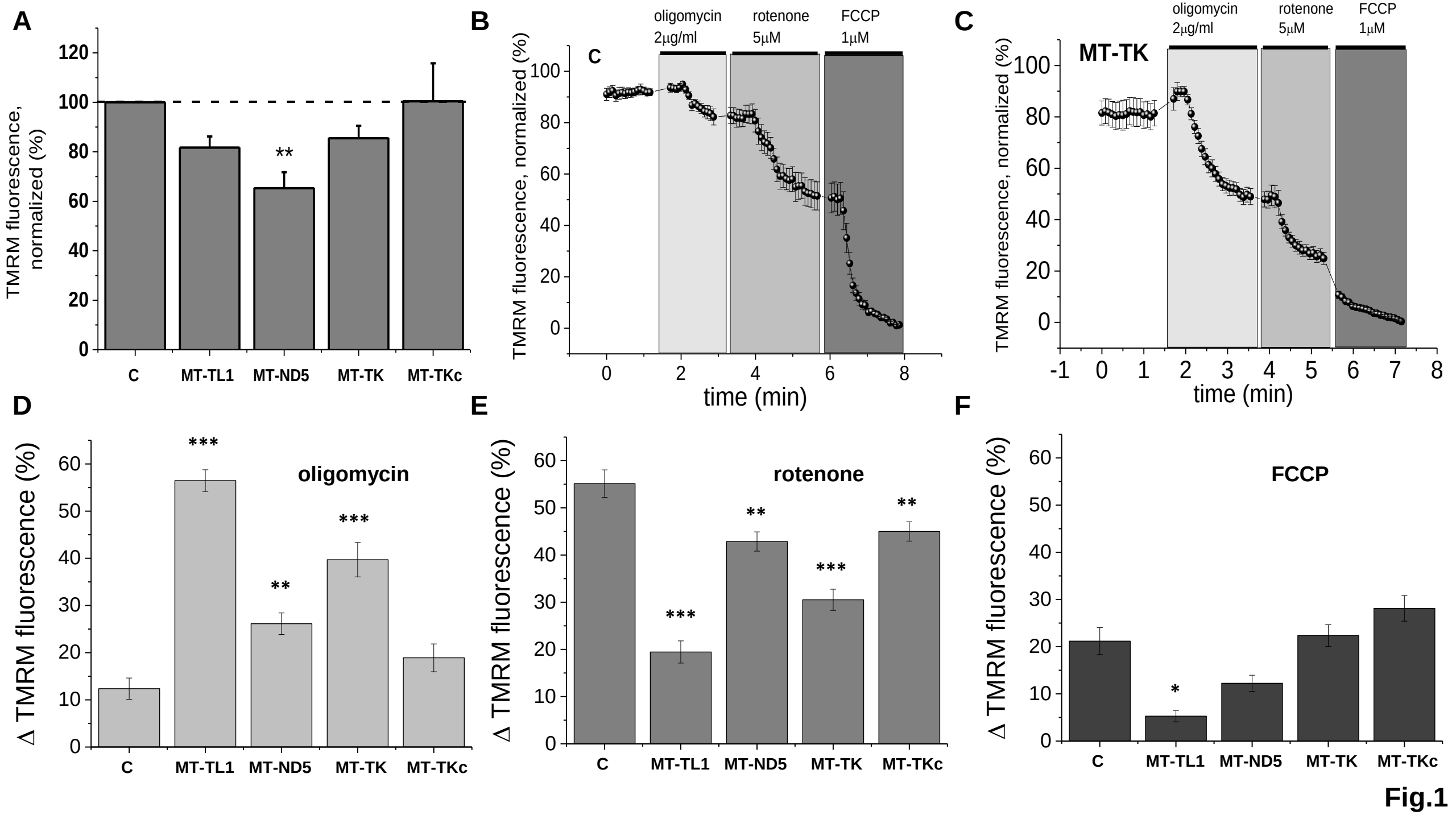
A
TMRM fluorescence, normalized (%)
120
100
80
60
40
20
0
**
C
MT-TL1
MT-ND5
MT-TK
MT-TKc
B
TMRM fluorescence, normalized (%)
oligomycin 2μg/ml
rotenone 5μM
FCCP 1μM
C
time (min)
C
MT-TK
oligomycin 2μg/ml
rotenone 5μM
FCCP 1μM
TMRM fluorescence, normalized (%)
time (min)
D
Δ TMRM fluorescence (%)
oligomycin
***
**
***
E
Δ TMRM fluorescence (%)
rotenone
***
**
***
**
F
Δ TMRM fluorescence (%)
FCCP
*

Fig.1

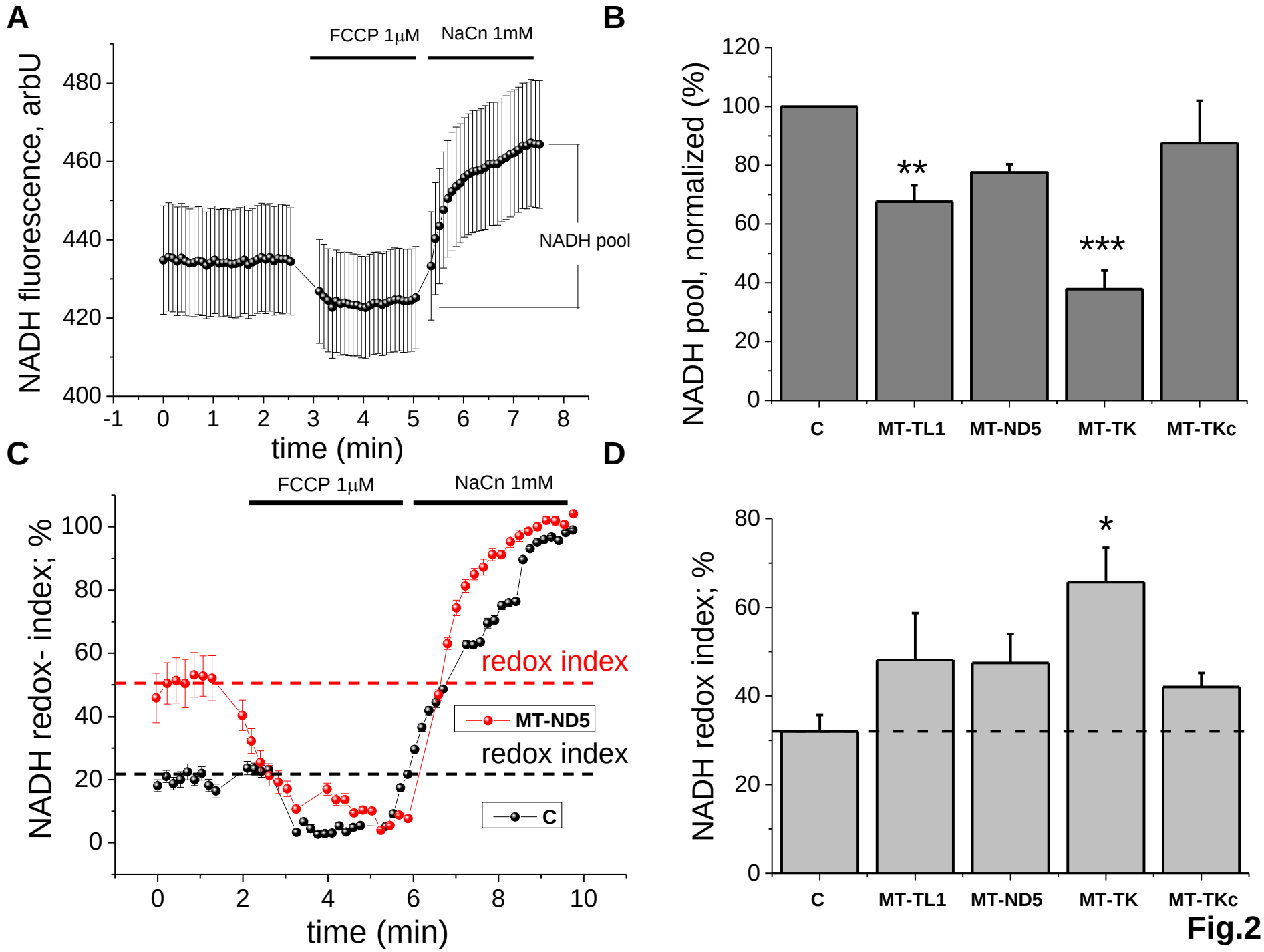
A
FCCP 1μM
NaCn 1mM
NADH fluorescence, arbU
480
460
440
420
400
-1
0
1
2
3
4
5
6
7
8
time (min)
NADH pool
B
NADH pool, normalized (%)
120
100
80
60
40
20
0
**
***
C
MT-TL1
MT-ND5
MT-TK
MT-TKc
C
FCCP 1μM
NaCn 1mM
NADH redox- index; %
100
80
60
40
20
0
redox index
MT-ND5
redox index
C
0
2
4
6
8
10
time (min)
D
NADH redox index; %
80
60
40
20
0
*
C
MT-TL1
MT-ND5
MT-TK
MT-TKc

Fig.2

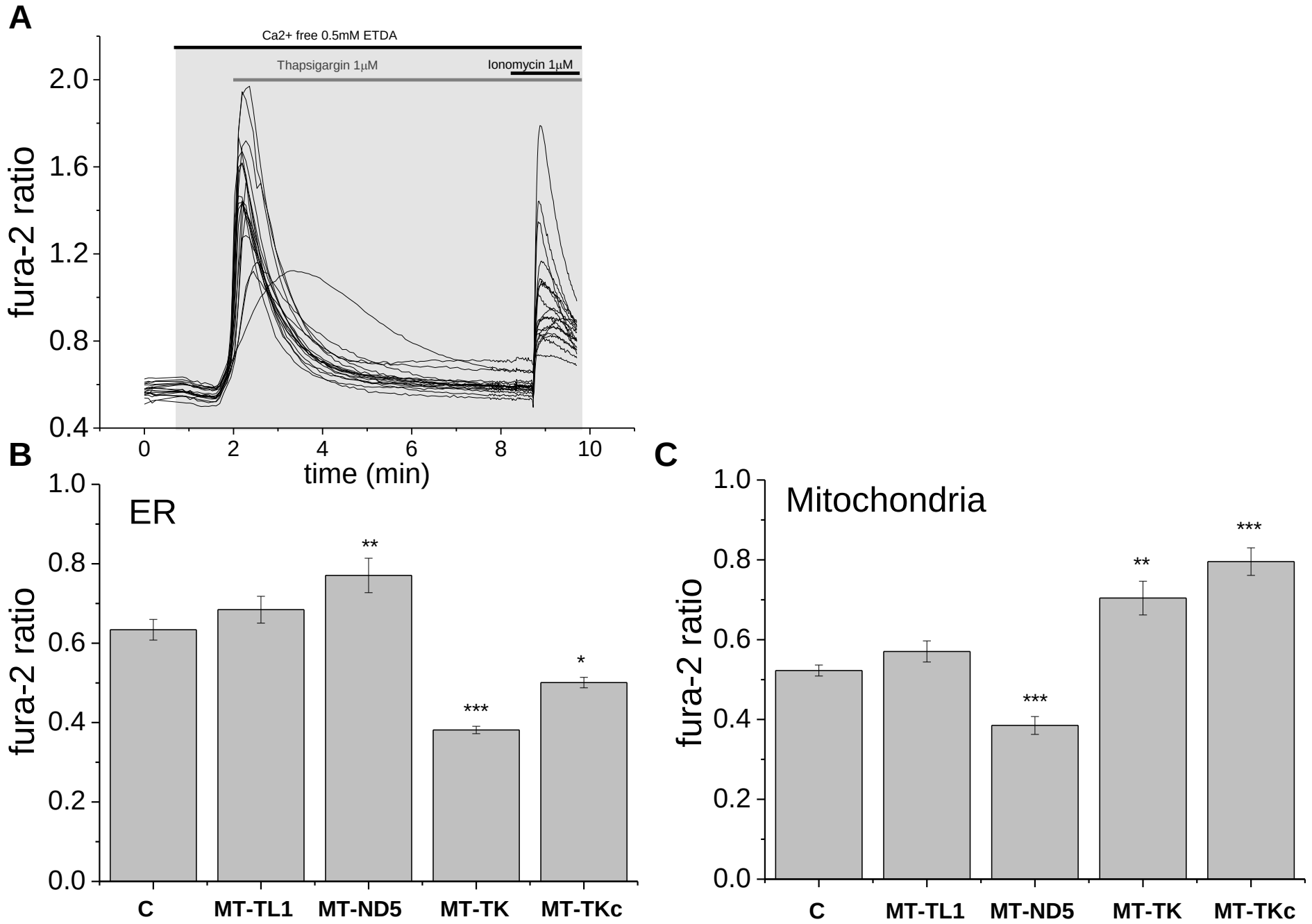
A
Ca2+ free 0.5mM ETDA
Thapsigargin 1μM
Ionomycin 1μM
fura-2 ratio
time (min)
B
ER
fura-2 ratio
C
MT-TL1
MT-ND5
MT-TK
MT-TKc
C
Mitochondria
fura-2 ratio
MT-TL1
MT-ND5
MT-TK
MT-TKc

Fig.3

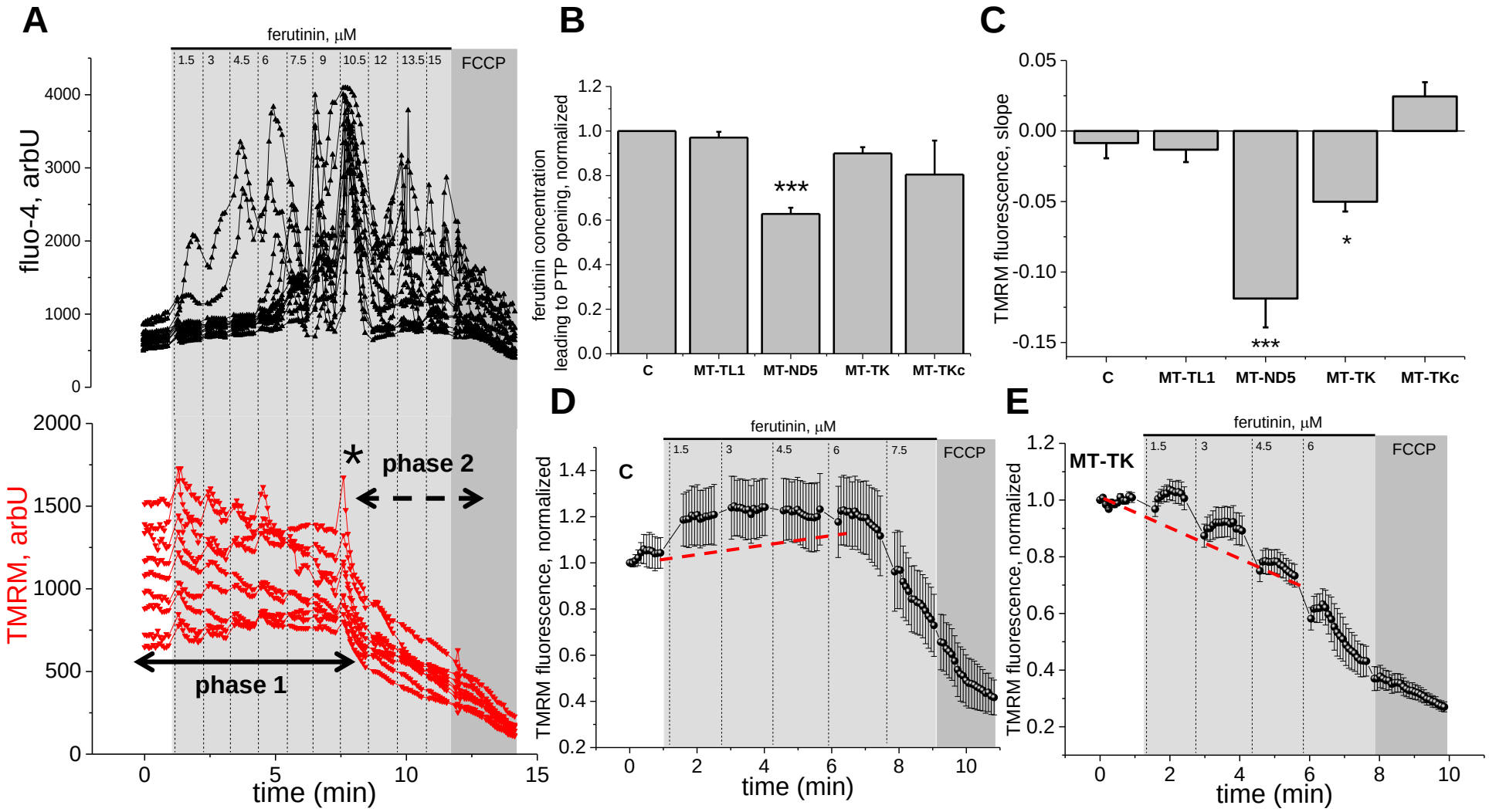
A
ferutinin, μM
1.5
3
4.5
6
7.5
9
10.5
12
13.5
15
FCCP
fluo-4, arbU
TMRM, arbU
phase 1
phase 2
time (min)
B
ferutinin concentration leading to PTP opening, normalized
***
C
MT-TL1
MT-ND5
MT-TK
MT-TKc
C
TMRM fluorescence, slope
***
*
D
ferutinin, μM
C
TMRM fluorescence, normalized
time (min)
E
MT-TK
ferutinin, μM
TMRM fluorescence, normalized
time (min)

Fig.4

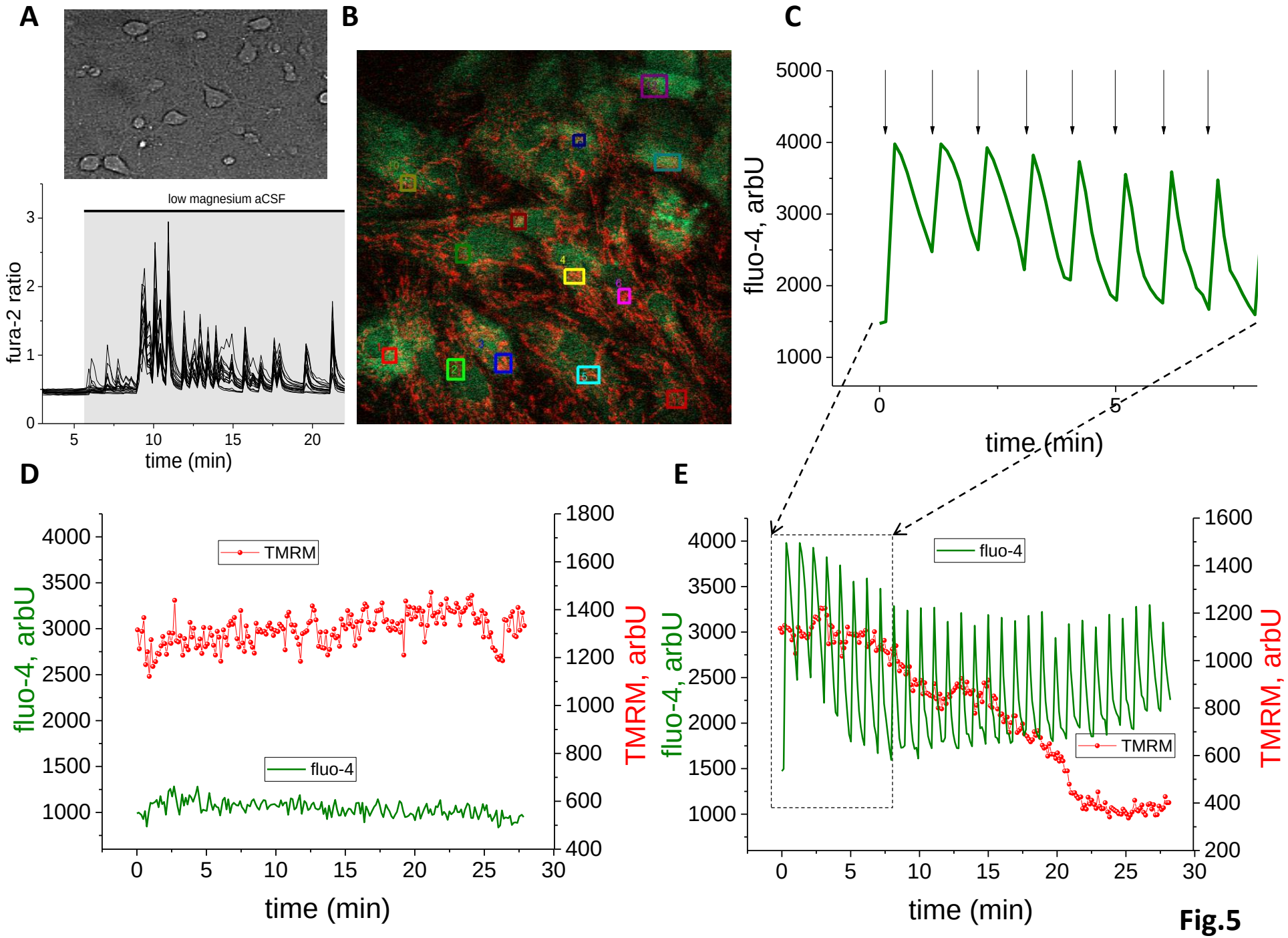
A
B
C
low magnesium aCSF
fura-2 ratio
time (min)
fluo-4, arbU
time (min)
D
TMRM
fluo-4
fluo-4, arbU
TMRM, arbU
time (min)
E
fluo-4
TMRM
fluo-4, arbU
TMRM, arbU
time (min)

Fig.5

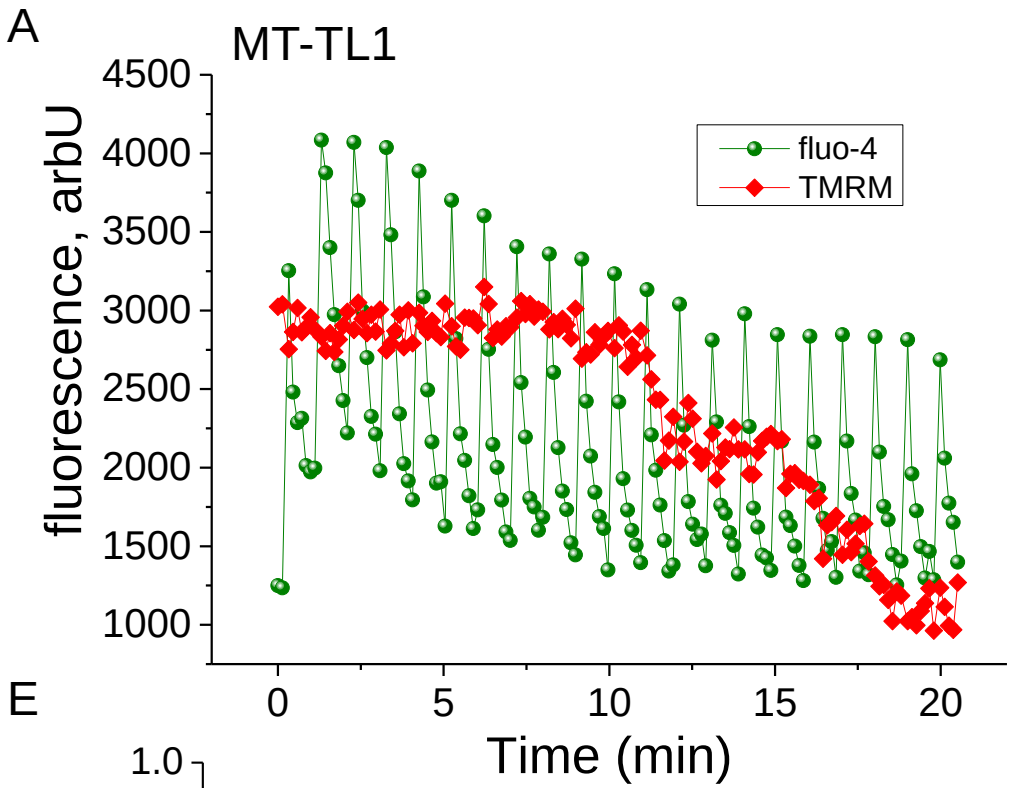
A
MT-TL1
fluorescence, arbU
fluo-4
TMRM
Time (min)

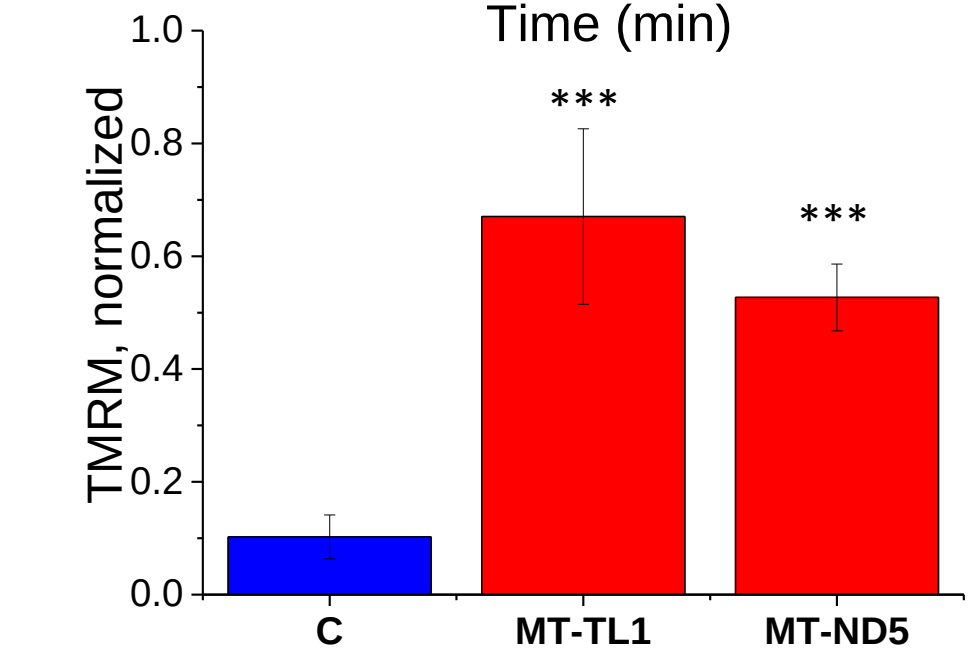
E
TMRM, normalized
***
***
C
MT-TL1
MT-ND5

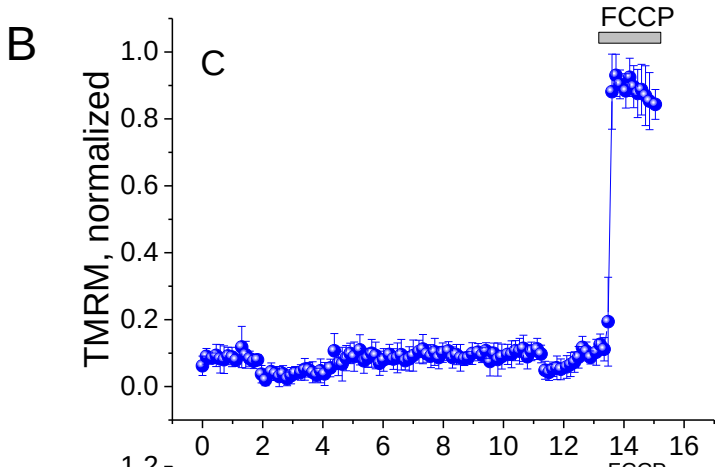
B
C
FCCP
TMRM, normalized
time (min)

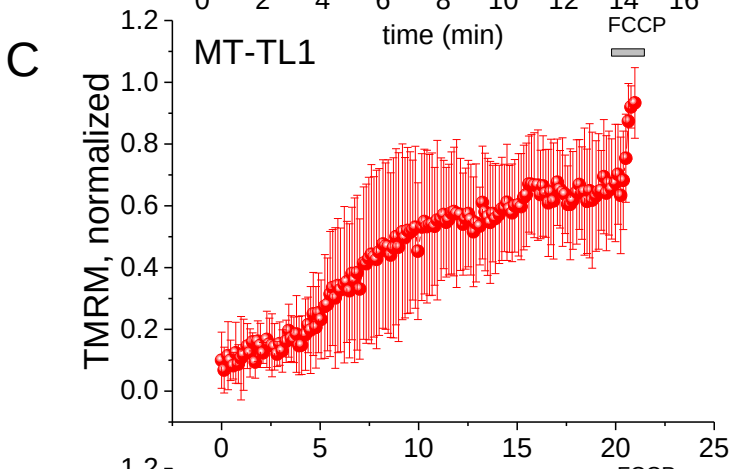
C
MT-TL1
FCCP
TMRM, normalized
time (min)

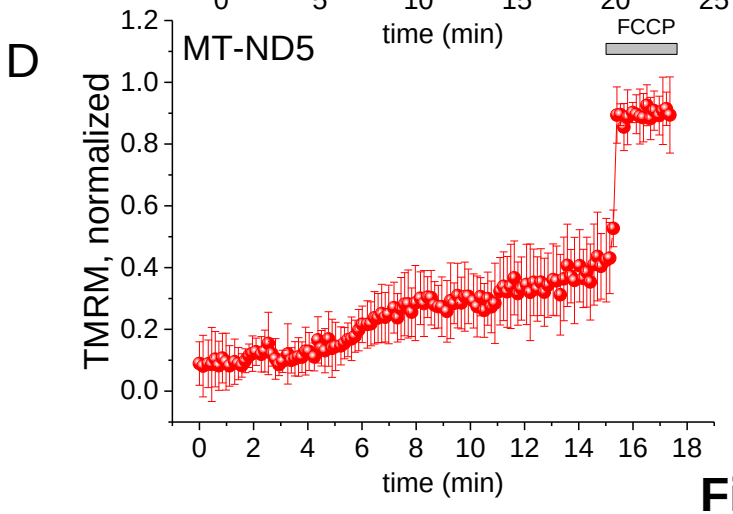
D
MT-ND5
FCCP
TMRM, normalized
time (min)

Fig.6

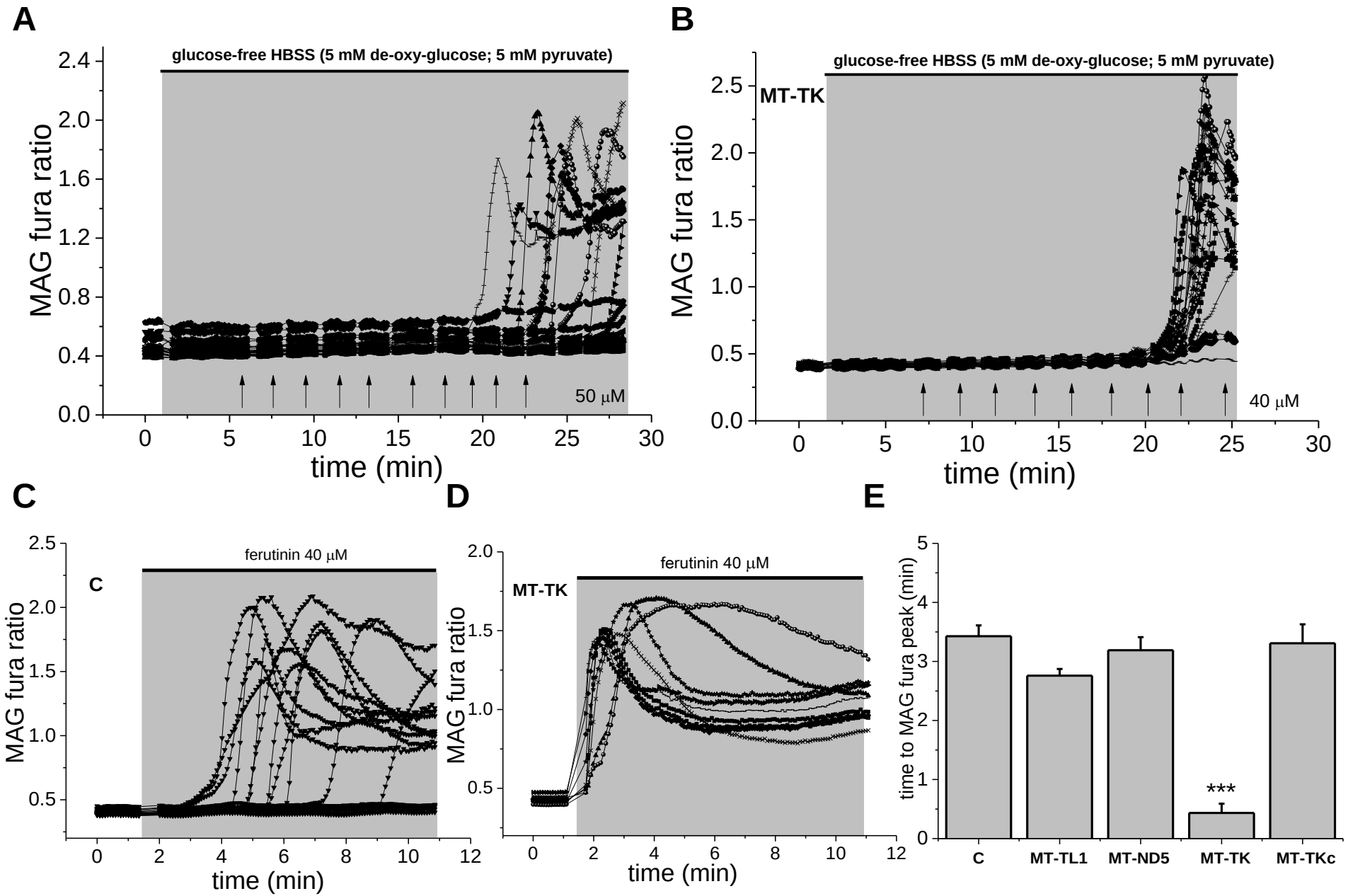
A
glucose-free HBSS (5 mM de-oxy-glucose; 5 mM pyruvate)
MAG fura ratio
time (min)
50 μM
B
glucose-free HBSS (5 mM de-oxy-glucose; 5 mM pyruvate)
MT-TK
MAG fura ratio
time (min)
40 μM
C
ferutinin 40 μM
C
MAG fura ratio
time (min)
D
ferutinin 40 μM
MT-TK
MAG fura ratio
time (min)
E
time to MAG fura peak (min)
***
C
MT-TL1
MT-ND5
MT-TK
MT-TKc

Fig.7

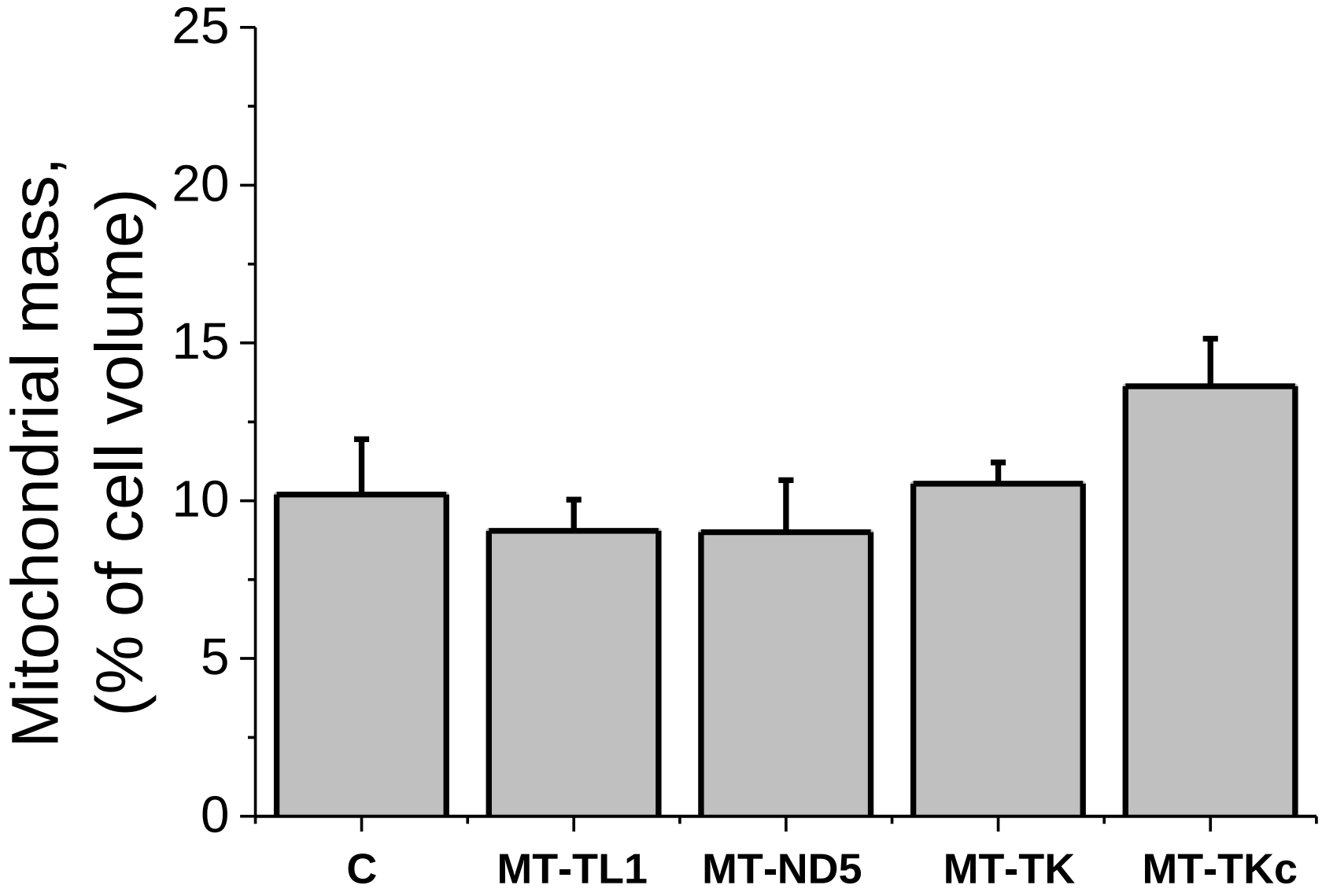
Mitochondrial mass,
(% of cell volume)
25
20
15
10
5
0
C
MT-TL1
MT-ND5
MT-TK
MT-TKc

Suppl. Fig.1